High-pressure Raman and FTIR studies of solid potassium, rubidium and caesium hydroxides

1994 J. Phys.: Condens. Matter 6 9789

(http://iopscience.iop.org/0953-8984/6/45/028)

J. Phys.: Condens. Matter 6 (1994) 9789–9806. Printed in the UK

High-pressure Raman and FTIR studies of solid potassium, rubidium and caesium hydroxides

M P Krobok and W B Holzapfel
Fachbereich Physik, Universität-GH-Paderborn, 33095 Paderborn, Germany

Received 10 May 1994, in final form 6 September 1994

Abstract. Effects of compression on the Raman and IR modes of KOH(D), RbOH(D) and CsOH(D) have been measured at pressures up to 20 GPa and temperatures down to 100 K using the diamond anvil technique. For all three hydroxides an ordering transition into the respective hydrogen-bonded low-temperature phases was found below 1 GPa at room temperature. In addition, the spectra of KOH(D) and RbOH(D) show significant changes at pressures above 6.5 GPa, which point to the existence of a new phase. The decrease in frequency of the IR- and Raman-active O–H(D) stretching vibrations with increasing compression indicates that hydrogen bonds exist also in the new high-pressure phase VI. The variation of the O–O distance at the phase transition IV ⇒ VI is estimated by using a double-minimum potential.

1. Introduction

The hydroxides of sodium, potassium, rubidium and caesium as well as their deuterated analogues show various polymorphic transformations at ambient pressure [1, 2]. At temperatures around 600 K a pseudo rocksalt structure (phase I) with space group $Fm3m$ is observed due to rapid reorientation of the hydroxide ions. At temperatures around 540 K, NaOH(D), KOH(D) and RbOH(D) transform into the same monoclinic structure type ($P2_1/m$) (phase II) while CsOH(D) transforms into an orthorhombic structure (Cm cm) (phase III). Metal–oxygen double layers are formed thereby while the protons become localized and take either of two positions adjacent to a particular oxygen atom. The protons (deuterons) rapidly jump back and forth between the two energetically equivalent positions. For NaOH(D) an additional transformation into the orthorhombic structure of the room-temperature phase III is observed at about 514 K [3].

Below room temperature, the alkali metal hydroxides, except NaOH, adopt structures with hydrogen-bonded O–H(D)···O–H(D)... zigzag chains [4–8]. For KOH(D), the monoclinic low-temperature phase is shown in figure 1 [9]. With respect to the orientation of the zigzag chains, various modifications exist. KOH(D) and CsOH(D) show antiferroelectric order in their respective phases IVa ($P2_1/n$), IVc ($P2_12_12_1$ or $Pnma$) while RbOH(D) exhibits ferroelectic order in its phase IVb ($Cmc2_1$).

Recently, it was noticed that below 250 K application of high pressure causes NaOH to transform into an antiferroelectric monoclinic structure with hydrogen bonded O–H···O–H... chains [10]. This phase is equivalent to the low-temperature phase of NaOD and KOH(D), respectively, at ambient pressure. For both NaOH and NaOD there exists at room temperature above 1 GPa another high-pressure phase V [11, 12].

In the present work, the Raman and FTIR spectra of potassium, rubidium and caesium hydroxides are studied over a wide range in pressure and temperature and in particular the changes occuring at the newly discovered IV–VI phase transition will be discussed.

0953-8984/94/459789+18$19.50

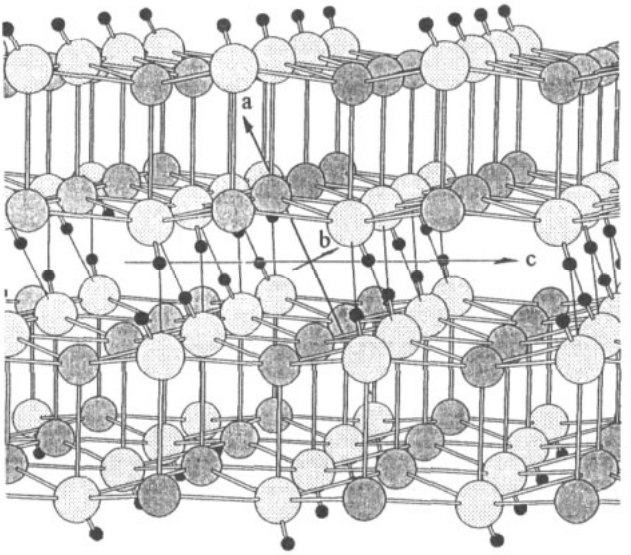

Figure 1. The monoclinic $P2_1/n$ structure of KOH(D) (phase IVa) at ambient pressure and 100 K (grey: O; dark grey: K; black: H(D)). The K–O double layers are linked by alternating hydrogen bonds.

2. Experimental technique

The KOH samples were prepared by drying KOH pellets ('ultrapure', Johnson Matthey Alfa Products) in vacuum at 500 K. KOD was prepared in a similar manner from a 40 wt% solution of KOD in D_2O (99.8% D, Aldrich Chemicals) by successive dehydration.

Due to the extremely hygroscopic character of anhydrous rubidium and caesium hydroxides special procedures are required for these materials. H Jacobs (University Dortmand) therefore provided the samples of RbOH and CsOH and their deuterated analogues which were prepared by conversion of the corresponding hydroxide hydrates using the respective amides in an autoclave [6, 7].

To avoid contamination by CO_2 and water, all samples were loaded into gasketed diamond anvil cells at liquid-N_2 temperature under a dry nitrogen atmosphere. For Raman experiments, Inconel gaskets of about 80 μm thickness with 200 μm holes were used. Best results have been obtained by compressing the samples without the use of a pressure-transmitting medium. Due to the strong IR absorption of the hydroxides in FTIR measurements only thin samples of about 30 μm thickness were used in 300 μm holes with nitrogen as pressure-transmitting medium.

Pressure inside the sample spaces was measured by the ruby fluorescence method using the linear ruby scale with $d\nu/dp = 7.53$ cm^{-1} GPa^{-1} and pressure-independent thermal corrections [13].

Raman spectra were excited with the 514.4 nm line of an argon-ion laser and measured at temperatures of about 100 K and 293 K. Temperatures of 100 K were obtained with a liquid-nitrogen-bath cryostat. The backscattered light was analysed by a Spex 1402 double spectrometer. The spectral resolution of the Raman bands was approximately equal to 2 cm^{-1}[14]. All IR spectra were taken at 293 K with a Bruker IFS 113v Fourier transform spectrometer using a tungsten halogen lamp and a liquid-N_2-cooled InSb detector. The spectral resolution was 8 cm^{-1}.

3. Results

3.1. Potassium hydroxide

Figure 2 shows typical Raman spectra of KOH in the O–H stretching region at ambient pressure (room temperature and 100 K, respectively). Due to the fact that the monoclinic room-temperature phase II ($P2_1/m$) of potassium hydroxide is centrosymmetric with two KOH(D) formula units per unit cell, only one Raman-active O–H(D) stretching mode can be observed. The unusually large halfwidth of the single vibrational band is a consequence of the dynamic disorder of the hydroxide ions. At temperatures below 233 K (KOD: 251 K) the orientations of the hydoxide ions are fixed by hydrogen bonds and antiparallel orientated O–H(D)···O–H(D)... chains are formed (figure 1). Due to the doubling of the unit cell the Raman line of the stretching mode splits into a symmetric (A_g) and an antisymmetric (B_g) component in the transformation to the monoclinic phase IVa ($P2_1/n$), where also a small jump to lower wavenumbers is noticed.

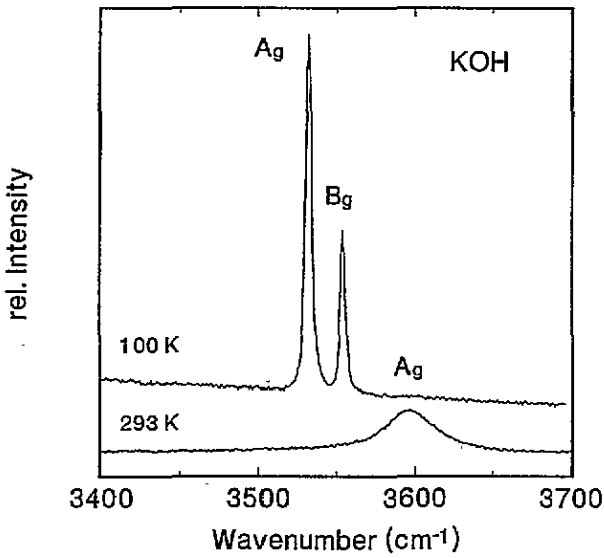

Figure 2. Ambient-pressure Raman spectra of the O–H stretching modes of KOH at room temperature and 100 K.

Figure 3 shows Raman spectra in the O–H stretching region of KOH at 293 K under various pressures. At about 1 GPa, a first phase transition is noticed by a splitting of this vibrational mode. This transformation can be easily traced back to the transition from the room-temperature phase II to the hydrogen-bonded low-temperature phase IVa at ambient pressure. With increasing compression, the O–H(D) stretching modes shift almost linearly to lower frequencies. The decrease in wavenumbers of these modes upon compression is usually regarded as an indication of increasing strength of hydrogen bonding. This leads to the conclusion that pressure mainly reduces the interlayer distances of the monoclinic phase with a decrease in the O–O distances along the planar zigzag chains of oxygen atoms. With further compression a second phase transition was observed in the Raman spectra beginning at 6.2 GPa. The spectra of the symmetric and antisymmetric modes vanish while two new lines appear about 40 cm^{-1}above the initial value. However, since neither the intensity nor

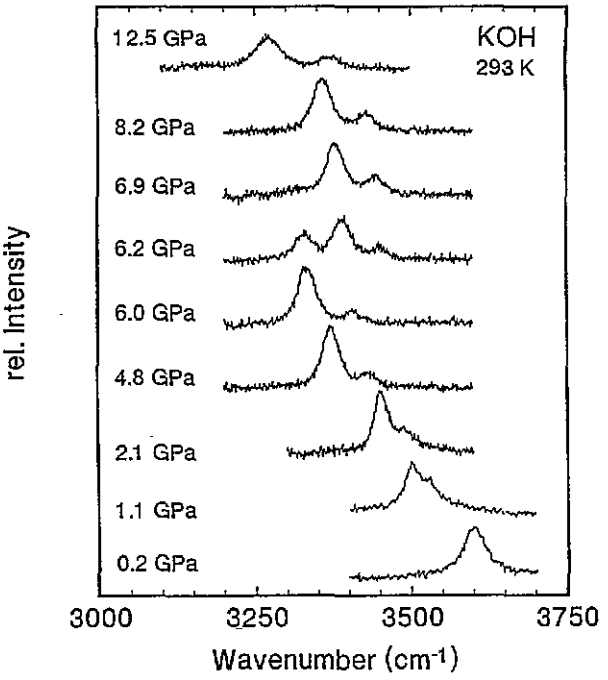

Figure 3. Raman spectra of KOH of the stretching modes at 293 K and different pressures.

the frequency distance of the lines is influenced by the transformation, the new modes can be assigned again as symmetric and antisymmetric O–H(D) stretching vibrations. Above the transition pressure both lines show the same strong decrease in frequency with pressure. Therefore hydrogen bonding takes place also in the new phase which is called phase VI. Due to a dramatic broadening in experimental line width no further data have been collected above 15 GPa.

For KOH the pressure dependence of the wavenumbers for the O–H stretching modes at room and low temperature are shown in figure 4. Table 1 gives the results of linear fits to the data of both KOH and KOD. The isotope effect reduces the frequencies of the O–D stretching modes in KOD with respect to O–H in KOH by a nearly constant factor of 0.74 up to 15 GPa. With the exception of the phase transition II $\Rightarrow$ IVa at 1 GPa and 293 K the results for isothermal compression at 100 K and room temperature are equivalent.

IR spectra of KOH and KOD were recorded at 293 K in the frequency range of the O–H(D) stretching modes. Due to the drastic increase in the full width at half maximum (FWHM) of the fundamental absorption in KOH, the symmetric and antisymmetric stretching modes cannot be separated. The observed broadening in line width is primarily caused by increasing hydrogen-bond strength with compression, whereas materials without H bonds like NaOH [10] show sharp bands in the high-pressure IR spectra. More details can be seen in the IR spectra of KOD (figure 5). By its isotope shift, the fundamental O–D vibration appears in the range from 2400 cm^{-1} to 2700 cm^{-1}. Since the IR spectra in transmission measurements with a diamond anvil cell are obscured between 1800 cm^{-1} and 2800 cm^{-1} by two- and three-phonon absorption of the diamonds, the fundamental line of the IR-active OD stretching mode is particularly influenced. The second band in the spectra can be assigned as the stretching mode of the OH impurity in KOD. Due to the low concentration

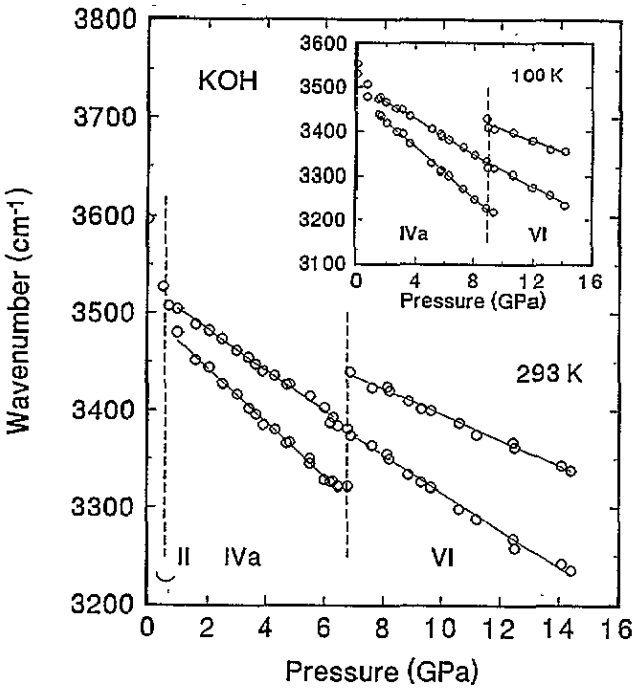

Figure 4. Effect of pressure on the stretching modes in KOH at room temperature and 100 K.

Table 1. Linear relations describing the effect of pressure on the IR and Raman frequencies in phase IVa and VI for KOH(D). $E(P) = E_0 + E'P$.

			KOH		KOD	
Phase	Temperature (K)		E_0 (cm^{-1})	E' ($\frac{cm^{-1}}{GPa}$)	E_0 (cm^{-1})	E' ($\frac{cm^{-1}}{GPa}$)
		IR	—	—	3510.3(41)	−25.6(10)
			3525.5(25)	−20.9(5)	2602.3(10)	−14.9(2)
	293		3500.0(20)	−28.1(5)	2583.7(23)	−19.0(3)
IVa		Raman	205.4(6)	14.1(2)	203.4(13)	13.8(3)
			164.5(3)	3.6(1)	163.4(5)	3.6(1)
			82.6(8)	−9.2(8)	79.8(10)	− 8.2(8)
	100	Raman	3506.0(20)	−19.8(3)	2577.6(20)	−11.4(3)
			3476.4(21)	−28.1(4)	2554.4(32)	−16.5(4)
		IR	—	—	3498.0(40)	−13.9(4)
			3529.0(30)	−13.3(5)	2586.3(51)	− 6.7(5)
	293		3508.1(40)	−19.3(5)	2586.0(21)	−12.6(2)
		Raman	204.6(29)	7.7(3)	202.5(68)	7.9(7)
VI			178.0(98)	4.7(11)	202.7(48)	2.0(5)
			118.8(36)	6.2(3)	117.1(35)	6.1(4)
			3532.0(18)	−12.7(15)	2573.2(30)	−10.8(3)
	100	Raman	3479.4(15)	−16.9(12)	2563.5(36)	− 4.5(2)

of OH ions in the material the O–H vibrations are uncoupled and not affected by factor group splitting or infrared band-broadening features such as for example TO/LO splittings of

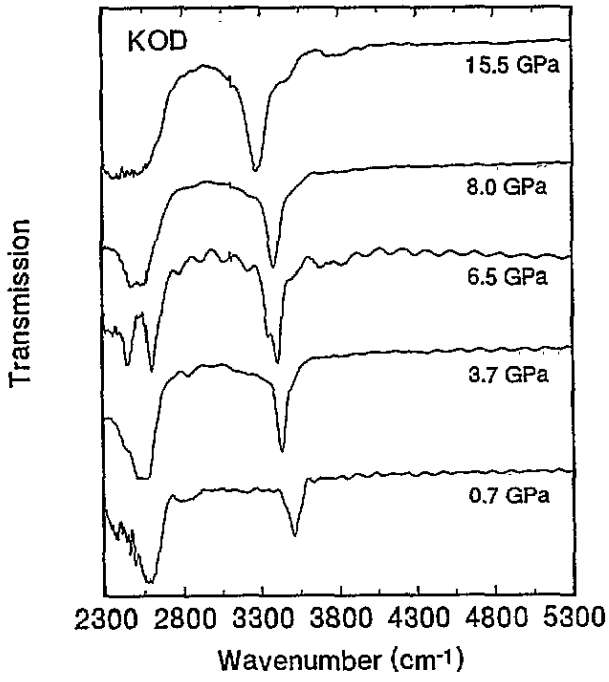

Figure 5. IR spectra of the stretching modes in KOD at room temperature and different pressures.

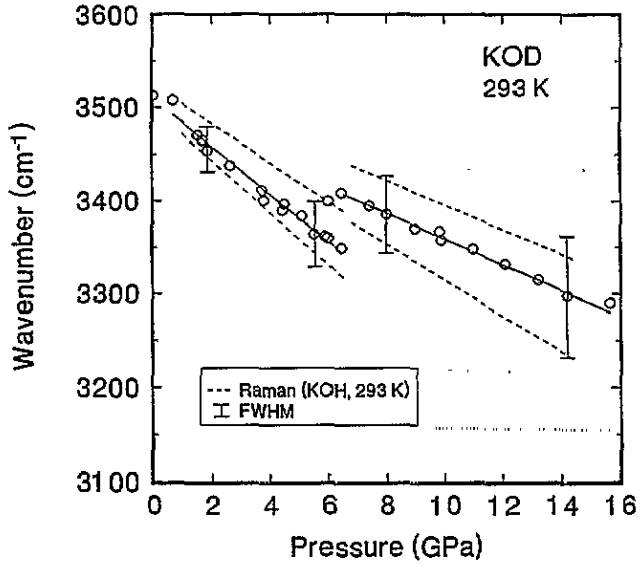

Figure 6. Effect of pressure on the IR-active O–H stretching mode in KOD.

phonon modes. The variation of the observed O–H line with pressure is shown in figure 6. The comparison with the corresponding symmetric and antisymmetric Raman lines of KOH shows clearly the local and uncoupled character of the single IR mode. Furthermore, the IR

band also shows an abrupt change in frequency in the pressure range of the phase transition IVa ⇒ VI.

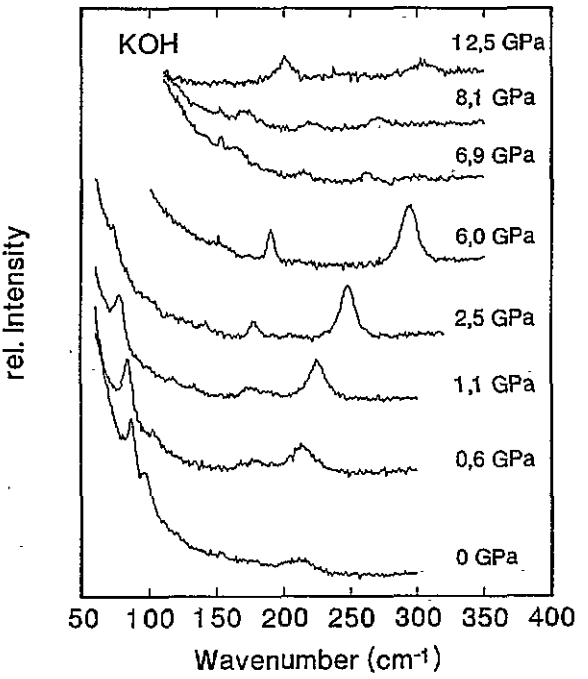

Figure 7. Raman spectra of KOH in the low-frequency range at room temperature and different pressures.

Significant changes occur also in the lattice modes of KOH(D) under pressure (figure 7). Up to 6 GPa two lines above 150 cm^{-1} increase in intensity while the other lines become broad and disappear in the backgroand. A tentative assignment of the bands in this frequency range can be made by analogy to an ambient-pressure normal-coordinate analysis of KOH(D) [15]. Accordingly the mode above 200 cm^{-1} is assigned to an internal K–O stretching vibration parallel to the *c*-axis (figure 1). The weak line near 180 cm^{-1} can be assigned to a K–O stretching mode perpendicular to the double layers but with more external character. In figure 8 the wavenumbers for these lattice modes are graphically represented as functions of pressure. It can be seen clearly that the low-energy translational mode below 100 cm^{-1} shows a tendency to soften with increasing pressure. This shear mode can be assigned to a vibration, where the two K–O planes of one double layer move against each other. The anomalous behaviour of the shear mode with compression is plausible if one considers that with increasing strength of hydrogen bonding a gliding of the layers upon each other occurs along the *c*-axis until the two layers are arranged one upon another. It should be mentioned here that for RbOH(D) and CsOH(D) this arrangement of the oxygen and alkali-metal ions already exists in the low-temperature phase at ambient pressure. As is seen in figure 7 drastic changes occur in the lattice modes at pressures of about 6 GPa, and the low-frequency spectra above these pressures are characterized by at least three very weak bands with a great deal of uncertainty regarding the assignment of these bands. Finally, no isotope effect can be observed in the lattice modes of KOD.

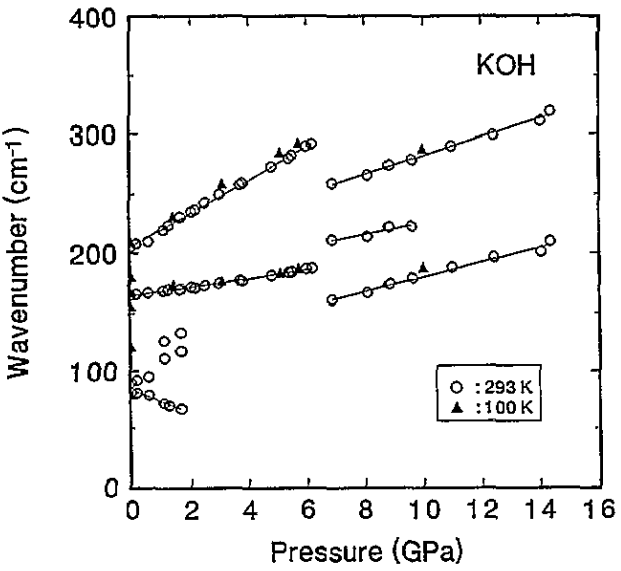

Figure 8. Effect of pressure on the low-frequency Raman modes of KOH at room temperature and 100 K.

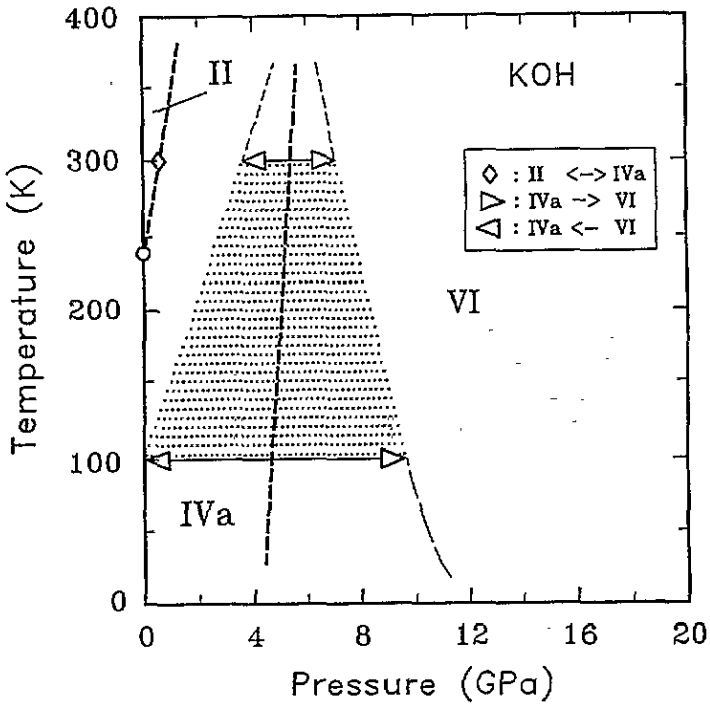

Figure 9. Pressure–temperature phase diagram of KOH.

The information on structural stabilities of the different phases of KOH under pressure as obtained from the given Raman and FTIR studies is illustrated in figure 9. Table 2 gives

Table 2. Transformation pressures at different temperatures for KOH(D) and RbOH(D).

		Compression		Decompression
	T (K)	p^a (GPa)	p^b (GPa)	p^c (GPa)
KOH	293	0.7(3)	6.7(5)	4.1(4)
	233[d]			
	100	—	9.0(5)	< 1.0
KOD	293	0.5(3)	6.8(5)	3.2(4)
	251[d]			
	100	—	9.8(6)	< 1.0
RbOH	293	0.8(3)	6.6(5)	3.5(5)
	265[d]			
	100	—	11.0(6)	1.5(4)
	300[d]			
RbOD	293	—	6.6(5)	3.4(4)

[a] Transition from phase II into phase IV.
[b] Transition from phase IV into phase VI.
[c] Reverse transition from phase VI into phase IV.
[d] Transition from phase II into phase IV at ambient pressure [5, 6, 9].

the observed transformation pressures for isothermal compression and decompression. In the phase diagram, the region of hysteresis for the phase transition IVa $\Leftrightarrow$ VI obtained by isothermal measurements with stepwise decreasing pressure is represented by shading. The equilibrium transition pressure can roughly be estimated by taking reasonable average values between the upward and downward transformation pressures as illustrated by the broken line in figure 9. From a comparison of the transformation pressures for KOH and KOD in table 2, one can see that the differences in the two phase diagrams are only marginal.

3.2. Rubidium hydroxide

At ambient pressure and low temperature the crystal structure IVb of RbOH is orthorhombic ($Cmc2_1$) with four formula units per unit cell [6]. This structure is essentially the same as the monoclinic structure IVa of KOH(D), except that for RbOH(D) adjacent hydrogen bonded O–H(D)$\cdots$O–H(D)... chains are ferroelectrically ordered. In the Raman spectra of this low-temperature phase the symmetric (A_1) and antisymmetric (B_2) O–H streching modes can be assigned [16]. Above 265 K (RbOD: 300 K) rubidium hydroxide crystallizes in a monoclinic $P2_1/m$ structure with $Z = 2$. The large halfwidth of the single O–H mode in the Raman spectrum points to a large dynamic disorder of the protons in this paraelectric phase.

Two phase transitions were detected in RbOH on compression at room temperature. Already below 1 GPa the phase transition from the monoclinic room-temperature phase II to the hydrogen-bonded low-temperature phase IVb can be observed. At this transition, a new line appears about 70 cm^{-1} below the initial value. Under further compression, the single line splits into a symmetric (A_1) and an antisymmetric (B_2) vibrational component, both with a strong decrease in frequency with increasing pressure. At about 6.6 GPa a second phase transition can easily be identified by a jump of the O–H stretching modes to higher wavenumbers, which is characteristic for the transformation into the high-pressure phase VI of KOH(D). However, the energy differences of the stretching vibrations at the phase transition IV $\Rightarrow$ VI in the case of RbOH ($\Delta_{A_1} = 198$ cm^{-1} and $\Delta_{B_2} = 143$ cm^{-1}) are remarkably larger than for KOH ($\Delta_{A_1} = 107$ cm^{-1} and $\Delta_{B_2} = 91$ cm^{-1}). In figure 10

the wavenumbers of the O–H stretching modes of RbOH are graphically represented as functions of pressure. Above 1 GPa the spectra at 100 K show no significant differences with respect to the room temperature spectra except that the phase transition IVb ⇒ VI occurs at slightly higher pressures.

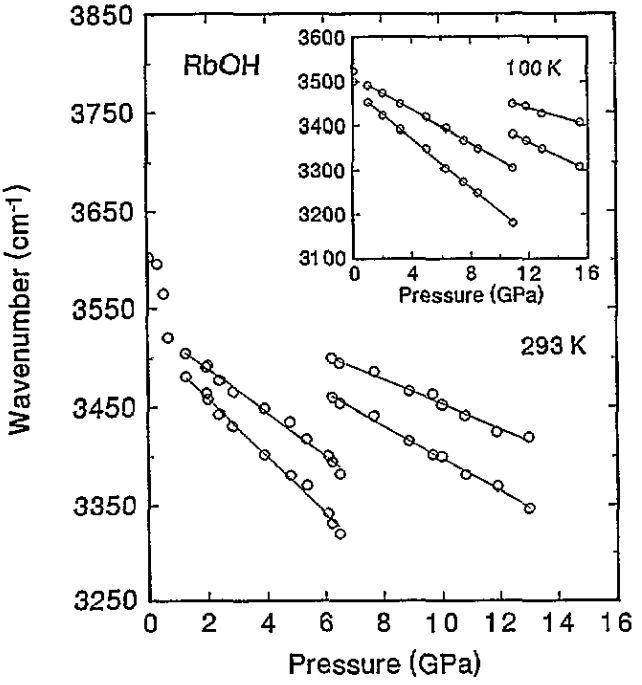

Figure 10. Effect of pressure on the stretching modes in RbOH at room temperature and 100 K.

FTIR transmission spectra of RbOD in the wavenumber range of interest were recorded up to 16 GPa. The strong mode at about 3400 cm^{-1}, caused by the OH impurity in RbOD, shifts due to the hydrogen bonding to lower values with increasing pressure. In the spectra for the phase mixture recorded around 7 GPa the phase transition IVb ⇒ VI can clearly be seen by two absorption bands, one of phase IVb and one of phase VI, respectively. Figure 11 shows the variation of the observed O–H line with pressure and table 3 summarizes the results of linear fits to the Raman and IR data. Despite the comparatively large line width the uncoupled IR mode can be localized always between the corresponding Raman lines.

To get more information about the properties of rubidium hydroxide, Raman spectra in the range of the lattice modes were collected at various pressures and temperatures. The results of these measurements are shown in figure 12. First of all the intensity of the Raman scattering peaks increases with increasing pressure beyond the phase transition II ⇒ IVb at about 1 GPa. An assignment of the two strongest bands can be made by analogy to KOH(D) and accordingly the mode above 200 cm^{-1} is assigned to an internal Rb–O stretching vibration parallel to the double layers and the small line near 100 cm^{-1} to an Rb–O stretching mode perpendicular to the layers. As can be seen in figure 12, all lattice modes shift to higher frequencies with pressure. Beyond the phase transition IVb ⇒ VI at 7 GPa the Raman spectra are dramatically altered.

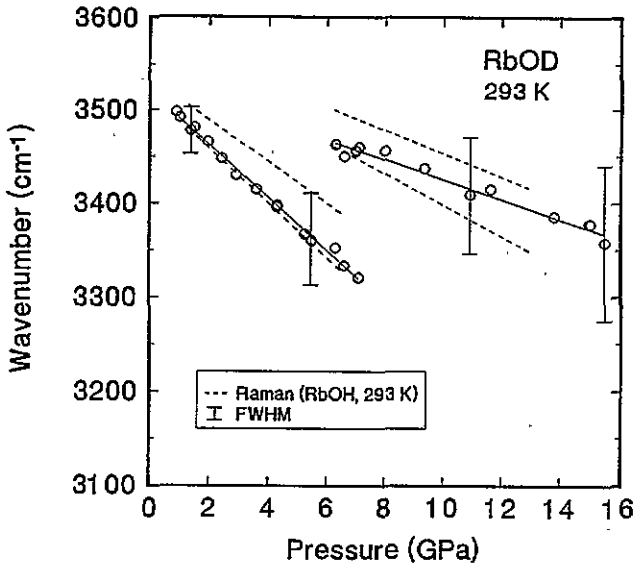

Figure 11. Effect of pressure on the IR-active O–H stretching mode in RbOD.

Table 3. Linear relations of the IR and Raman frequencies in phases IVa and VI for RbOH(D). $E(P) = E_0 + E'P$.

			RbOH		RbOD[a]	
Phase	Temperature (K)		E_0 (cm^{-1})	E' ($\frac{cm^{-1}}{GPa}$)	E_0 (cm^{-1})	E' ($\frac{cm^{-1}}{GPa}$)
		IR	—	—	3518.2(20)	−28.1(6)
			3533.0(30)	−22.1(7)	—	—
	293		3517.2(31)	−29.2(8)	—	—
IVb		Raman	176.0(10)	14.1(4)	—	—
			105.7(7)	3.4(2)	—	—
			52.0(10)	2.5(3)	—	—
			3511.1(20)	−18.8(2)	—	—
	100	Raman	3480.0(30)	−27.4(4)	—	—
		IR	—	—	3531.2(70)	−10.6(7)
			3578.1(62)	−12.5(6)	—	—
VI	293	Raman	3565.0(40)	−16.7(4)	—	—
			183.7(73)	6.3(7)	—	—
			3554.0(120)	− 9.5(9)	—	—
	100	Raman	3551.0(41)	−15.6(3)	—	—

[a] In RbOD the Raman lines were too weak for registration.

As a result of the Raman and FTIR measurements of rubidium hydroxide, the observed transformation pressures for isothermal compression and decompression are listed in table 2. The behaviour of the O–H(D) stretching modes was used as a criterion for the back-transformation pressure. Since the quality of the Raman spectra dramatically decreases with decreasing pressure below 3 GPa at low temperatures the back-transformation pressure at 100 K is quite uncertain. Interestingly, the transition pressures in RbOH(D) are very similar to those observed in KOH(D).

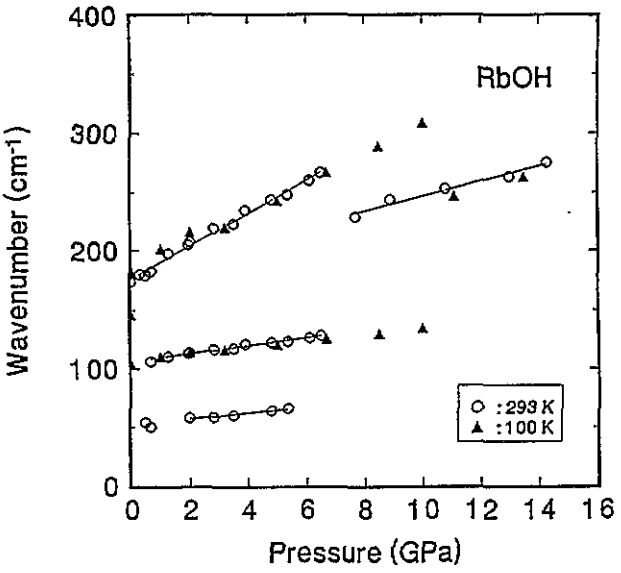

Figure 12. Effect of pressure on the low-frequency Raman modes of RbOH at room temperature and 100 K.

3.3. Caesium hydroxide

Finally, the results of Raman and FTIR measurements of CsOH(D) are presented. The room-temperature ambient-pressure phase (III) of CsOH(D) is orthorhombic (*Cm cm*) with four formula units per unit cell and dynamically disordered hydroxide ions [17]. A second orthorhombic modification (IVc) is well known at low temperatures. For this phase, two different space groups were suggested, one with $P2_12_12_1$ ($Z = 4$) [7] and one with *Pnma* ($Z = 4$) symmetry [8]. However, O–H(D)···O–H(D)... zigzag chains are formed in both cases with parallel alignments within each layer and with opposite alignments in adjacent layers. Infrared and Raman studies on CsOH at ambient pressure have exhibited that the essential features of the spectra are the same as in the case of KOH(D) and RbOH(D) [16].

Raman spectra of CsOD in the stretching region under various pressures show a splitting of the single O–D line of phase III at the transition to phase IVc at about 1 GPa. The resulting symmetric and antisymmetric stretching modes exhibit a strong red shift with increasing pressure. In figure 13 the wavenumbers of these bands are plotted as a function of pressure and the results of linear fits are given in table 4. In contrast to the high-pressure behaviour of KOH(D) and RbOH(D) no evidence could be found for a further phase transition up to 11 GPa. Moreover, the continuous shift of the single infrared-active O–H band in CsOD shown in figure 14 gives no sign of any further phase transition up to 25 GPa.

The results for room-temperature Raman measurements of the lattice modes support these observations on the structural behaviour of CsOH(D). Three lines can be observed up to 15 GPa. The pressure dependence of the wavenumbers for these modes together with the results for 100 K are plotted in figure 15. As can be seen from a comparison with figures 8 and 12 these modes behave quite similarly to the ones reported for KOH(D) and RbOH(D) with the only difference for CsOH(D) being that the lattice vibrations are lower in frequency due to the larger mass of the caesium ion.

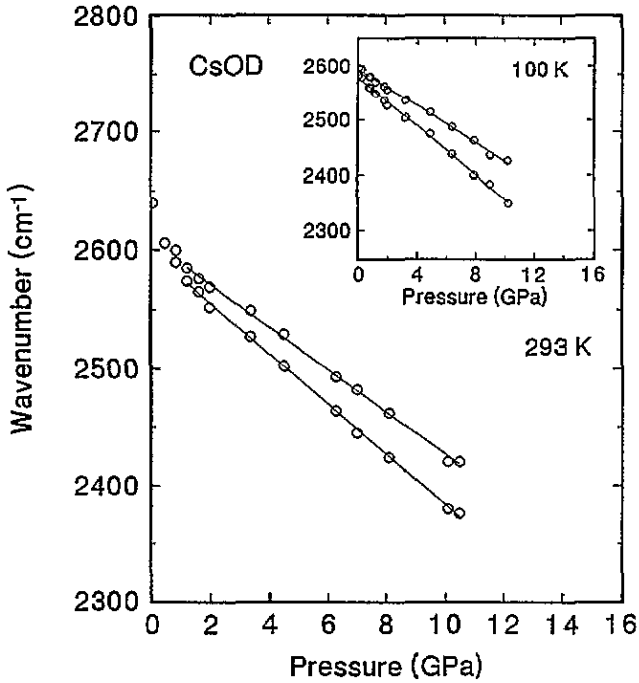

Figure 13. Effect of pressure on the stretching modes in CsOD at room temperature and 100 K.

Table 4. Linear relations of the IR and Raman frequencies in phase IVa and VI for CsOH(D). $E(P) = E_0 + E'P$.

			CsOH		CsOD	
Phase	Temperature (K)		E_0 (cm^{-1})	E' ($\frac{cm^{-1}}{GPa}$)	E_0 (cm^{-1})	E' ($\frac{cm^{-1}}{GPa}$)
		IR	3525.1(33)	−23.2(4)	3501.3(62)	−22.9(5)
			—[a]	—[a]	2607.5(23)	−18.1(3)
	293		—[a]	—[a]	2598.0(25)	−21.4(2)
IVc		Raman	157.0(22)	11.1(3)	147.0(20)	13.3(2)
			84.1(6)	3.2(1)	83.7(6)	4.1(1)
			56.7(16)	2.6(1)	47.1(12)	4.2(2)
			3528.0(10)	−21.7(2)	2594.0(20)	−16.9(3)
	100	Raman	3510.2(25)	−28.9(3)	2578.4(11)	−22.2(3)

[a] In CsOH the O–H Raman lines were too weak for registration at 293 K.

4. Discussion

The present Raman and FTIR measurements demonstrate clearly the presence of hydrogen bonds in KOH(D), RbOH(D) and CsOH(D) under pressure. By compression the O–H(D) distances are reduced and the hydrogen bonds are strengthened. This effect is documented mainly by the strong decrease in the frequencies of the O–H(D) bands [18]. In figure 16 the mean values of the symmetric and antisymmetric O–H stretching vibrations of the hydroxides under discussion are plotted. Below 9 GPa only a small deviation exists between the pressure dependence of the stretching modes in KOH, RbOH and CsOH. Thus, one can

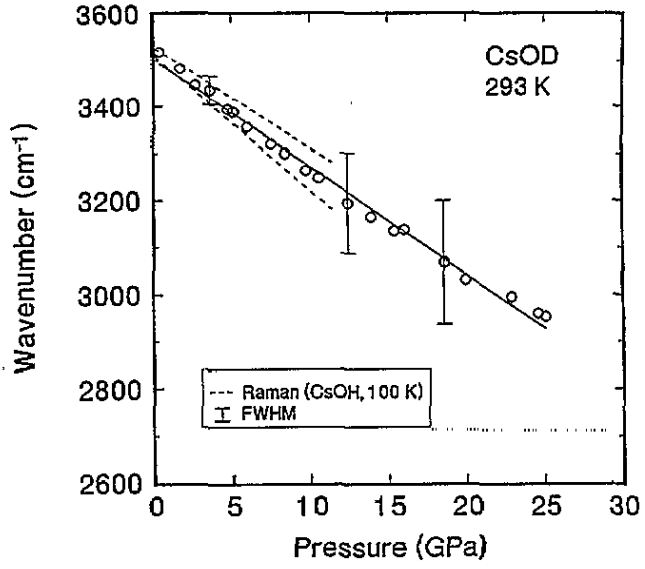

Figure 14. Effect of pressure on the IR-active O–H stretching mode in CsOD.

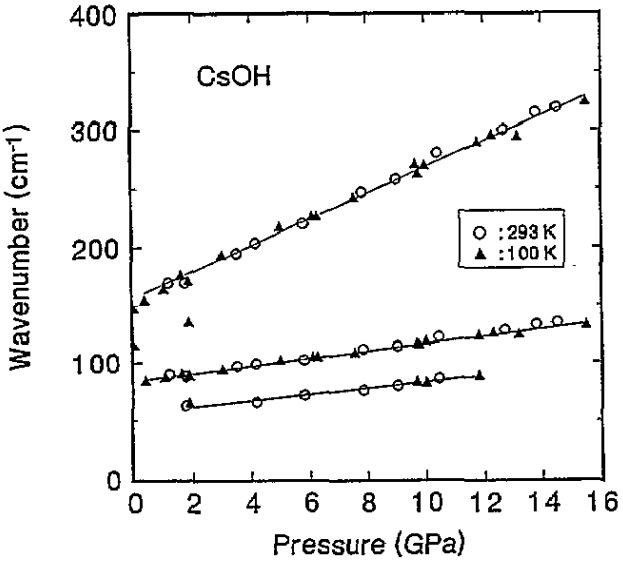

Figure 15. Effect of pressure on the low-frequency Raman modes of CsOH at room temperature and 100 K.

conclude that the variation of the O–O distance with pressure and thereby the variation of the interlayer distance has the same magnitude for all the hydroxides. At the transition to phase VI, the pressure dependence of the internal modes shows a large jump to higher frequencies for both KOH(D) and RbOH(D). Moreover, following the experimental results *it seems reasonable that hydrogen-bonded* O–H(D)···O–H(D)... *zigzag chains also exist in* the high-pressure phase VI. Thus, the frequency jump of the O– H(D) stretching modes to

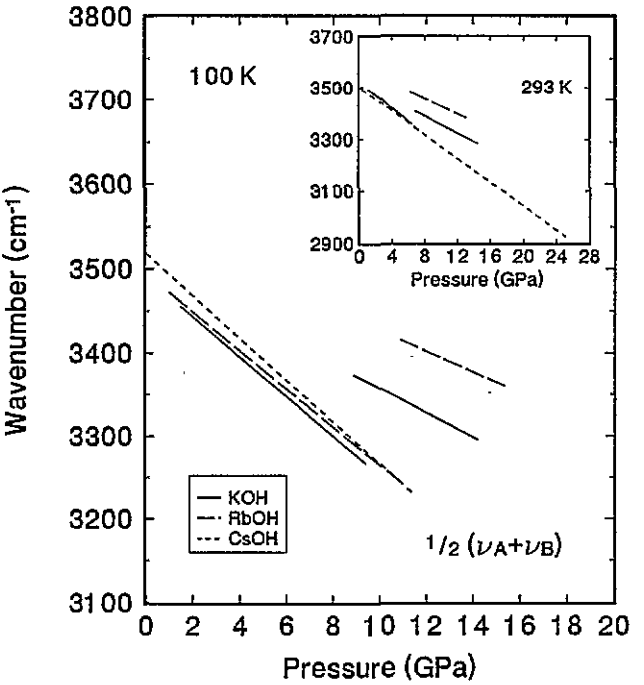

Figure 16. Pressure dependence of the mean values of the symmetric and antisymmetric O–H stretching modes for KOH, RbOH and CsOH at room temperature and 100 K.

higher values can be correlated with an increase of the O–O distance at this phase transition.

The variation of the O–O distance at the phase transition IV $\Rightarrow$ VI for KOH(D) and RbOH can be estimated by the use of a double Morse potential to describe a linear hydrogen-bonded O–H(D)$\cdots$O system [19,20]:

$$V = 2D_e\left[e^{-a(R-2r_0)}\cosh(2ar) - 2e^{-(1/2)a(R-2r_0)}\cosh(ar)\right].$$

Here, R is the O–O distance and r the distance between hydrogen and the centre of O–O. The constants r_0, D_e and a are model parameters and can be associated in first order with the equilibrium O–H(D) distance for a free hydroxyl, the bond dissociation energy and the bond strength, respectively. The vibrational energy can be calculated for the anharmonic double-minimum potential using perturbation theory [21]. For the first excitation energy the result can be written as

$$E_{0\to1} = \hbar\omega_e - \frac{1}{4.8}\frac{\hbar^2}{\mu^3\omega_e^4}\left[\frac{\partial^3 V}{\partial r^3}\right]_{r_e}^2 + \frac{1}{8}\frac{\hbar^2}{\mu^2\omega_e^2}\left[\frac{\partial^4 V}{\partial r^4}\right]_{r_e}$$

with

$$\omega_e^2 = \frac{1}{\mu}\left[\frac{\partial^2 V}{\partial r^2}\right]_{r_e}$$

where μ is the reduced mass, ω_e the classical oscillator frequency and r_e the equilibrium position for the proton. In order to determine the potential parameters r_0, D_e and a some

assumptions are usually made: (i) the correlation curve $\nu(\mathrm{OH(D)}) = f(R_{O\cdots O})$ should fit the known ambient-pressure frequency–distance relation for KOH(D), RbOH(D) and CsOH(D); (ii) since at ambient conditions the hydrogen bonding is comparatively weak in the hydroxides the curve should be flat in the region of the ambient pressure O–O distances; (iii) the calculated correlation curve should qualitatively agree with known empirical frequency-distance relations of O–H(D)···O groups in different compounds [22, 23] and especially with the high-pressure correlation data of ice [24]. As a result of the fit, the correlation curve of the O–D···O system is plotted in figure 17 and the corresponding potential parameters are listed in table 5. The offset between the empirical correlation and the fitted curve in this figure can be explained by the fact that the correlations given in the literature include data of many kinds of O–H(D)···O groups and therefore, the individual data points scatter widely.

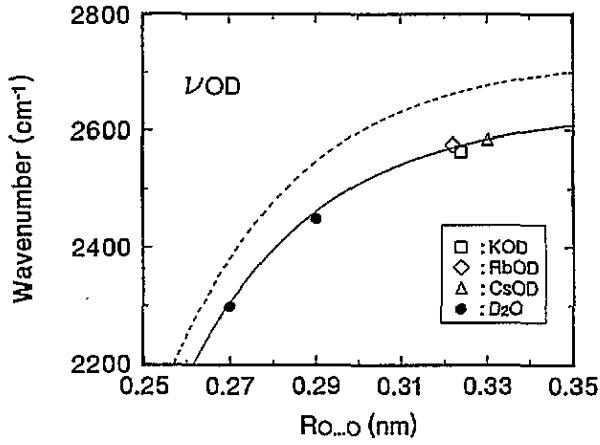

Figure 17. Frequency–distance diagram for a linear O–D···O system with ambient-pressure data for KOD, RbOD and CsOD. The broken curve represents the empirical correlation of Mikenda [22], the D_2O data are results of high-pressure Raman measurements on ice [24].

Table 5. Result of the parameter fit for the double-minimum potential.

	D_e (cm^{-1})	r_0 (nm)	a (nm^{-1})
OH···O	23 900	0.085	30
OD···O	23 200	0.084	30

One point should be mentioned with respect to the ambient-pressure frequency–distance relations. The double Morse potential is written for a linear hydrogen-bonded O–H(D)···O system. Actually in the hydroxides, the hydrogen bonds are more or less bent at ambient pressure [25]. For example, the value of the O–H(D)···O angle varies at low temperature from 163° for KOD [9] to 172° for CsOD [7]. On the other hand, it is evident from figures 4, 10 and 13 that the stretching modes are more sensitive below 1 GPa not only at room temperature but also in the hydrogen-bonded phases at 100 K. This can be explained by formation of linear hydrogen bonds with pressure. Therefore, to determine the potential

parameters, the known O–O distances are correlated with the extrapolated ambient pressure values for the O–H(D) stretching frequencies. The extrapolated values are between 50 cm^{-1} (KOD) and 5 cm^{-1} (CsOD) lower than the measured stretching frequencies.

Table 6. Variation of the O–O distance at the phase transition IV⇒VI for KOH(D) and RbOH.

	Pressure	$\nu_{OH(D)}$ (cm^{-1})		$R_{O...O}$ (nm)	
	(GPa)	IV	VI	IV	VI
KOH	9.0	3276(5)	3372(6)	0.285(3)	0.297(3)
KOD	9.8	2429(4)	2493(5)	0.285(3)	0.296(3)
RbOH	11.0	3239(5)	3414(6)	0.282(3)	0.304(3)

With the given correlation curve in figure 17 it is possible to estimate the variation of the O–O distance for KOH(D) and RbOH at the phase transition IV ⇒ VI. The results are presented in table 6. It can be seen that the oxygen distance increases by about 12 pm for KOH and 22 pm for RbOH. At this stage of the investigation it is not clear which mechanism is responsible for the IV–VI phase transition, but based on the facts that (i) hydrogen bonded O–H(D)···O–H(D)... chains exist in phase VI, (ii) the O–O distance increases and (iii) the volume decreases at the phase transition, a simple mechanism can be proposed. In phase IV, the dominant effect of pressure is to reduce the interlayer distance. However at the transition point, the repulsion forces of the Coulomb interaction between equal ions of adjacent double layers cause a rearrangement of the ions. One way to enlarge the distances, and therefore to reduce the repulsion forces between the oxygen ions and alkali-metal ions, respectively, is to glide the layers over each other parallel to the *c*-axis (figure 1). With the calculated variation of the O–O distance it is possible to estimate the amount of this shift. One can find a displacement of about 84 pm for KOH(D) and 113 pm for RbOH, for both cases not sufficient to place the oxygen ions directly above the alkali metal ions.

However, the very weak Raman spectra of the lattice modes in phase VI seems to indicate that not only a simple layer shift takes place at the phase transition IVa ⇒ VI, but also the arrangement of the ions within a double layer is affected. This supposition is supported by the fact that the phase transition is of first order with a considerable hysteresis.

Finally, a possible explanation is given for the observation that the IV–VI transition pressures in the hydroxides do not vary linearly with cationic radii. In contrast to RbOH(D) and CsOH(D), neighbouring double layers in KOH(D) are slightly displaced at ambient pressure. Based on the Raman spectra of the lattice modes (figures 7, 8) one can conclude that for KOH(D) not only is the interlayer distance reduced under compression in phase IV but also the layers glide over each other until they are arranged as in RbOH(D) and CsOH(D). Therefore, the observed phase transition IV–VI in KOH(D) is shifted to higher pressures with respect to RbOH(D).

Acknowledgments

We thank Professor H Jacobs (University of Dortmund) for providing the samples of RbOH(D) and CsOH(H) used in this study. This work was supported by the Deutsche Forschungsgemeinschaft (DFG) under grant No Ho486/19-2 .

References

[1] Smit J G, Dachs H and Lechner R E 1979 *Solid State Commun.* **29** 219
[2] Teichert W and Klemm W 1939 *Z. Anorg. (Allg.) Chem.* **243** 138
[3] Bleif H J and Dachs H 1982 *Acta Crystallogr.* A **38** 470
[4] White M A and More S A 1986 *J. Chem. Phys.* **85** 4629
[5] Bastow T J, Elcombe M M and Howard C J 1986 *Solid State Commun.* **59** 257
[6] Jacobs H, Mach B, Lutz H D and Henning J 1987 *Z. Anorg. (Allg.) Chem.* **544** 28
[7] Jacobs H, Mach B, Harbrecht B, Lutz H D and Henning J 1987 *Z. Anorg. (Allg.) Chem.* **544** 55
[8] Bastow T J, Elcombe M M and Howard C J *Solid State Commun.* **62** 149
[9] Mach B, Jacobs H and Schäfer W 1987 *Z. Anorg. (Allg.) Chem.* **553** 187
[10] Krobok M P, Johannsen P G and Holzapfel W B 1992 *J. Phys.: Condens. Matter* 4 8141
[11] Pistorius C W F T 1969 *Z. Phys. Chem., NF* **65** 51
[12] Beck H P and Lederer G 1993 *J. Chem. Phys.* **98** 7289
[13] Piermarini G J, Block S, Barnett J D and Forman R A 1975 *J. Appl. Phys.* **46** 2774
[14] Hirsch K R and Holzapfel W B 1981 *Rev. Sci. Instrum.* **52** 52
[15] Kanesaka I, Kawahara H and Kawai K 1984 *J. Raman Spectrosc.* **15** 165
[16] Lutz H D, Henning J, Jacobs H and Mach B 1986 *J. Mol. Struct.* **145** 277
[17] Henning J, Lutz H D, Jacobs H and Mach B 1989 *J. Mol. Struct.* **196** 113
[18] Lippincott E R and Schoeder R 1955 *J. Chem. Phys.* **23** 1099
[19] Holzapfel W B 1972 *J. Chem. Phys.* **56** 712
[20] Matsushita E and Matsubara T 1982 *Prog. Theor. Phys.* **67** 1
[21] Brüesch P 1982 *Phonons: Theory and Experiments I* (Berlin: Springer)
[22] Mikenda W 1989 *J. Mol. Struct.* **147** 1
[23] Novak A 1974 *Struct. Bonding* **18** 177
[24] Hirsch K R 1983 *Dissertation* Paderborn
[25] Chidambaram R and Sikka S K 1968 *Chem. Phys. Lett.* 2 162